—Original—

Virtual Monochromatic Imaging of Half-Iodine-Load, Contrast-Enhanced Computed Tomography with Deep Learning Image Reconstruction in Patients with Renal Insufficiency: A Clinical Pilot Study

Shingo Harashima[1†], Rika Fukui[1†], Wakana Samejima[1†], Yuta Hirose[1†], Toshiya Kariyasu[1*], Makiko Nishikawa[1†], Hidenori Yamaguchi[1,2†] and Haruhiko Machida[1*]

[1]Department of Radiology, Tokyo Women's Medical University Adachi Medical Center, Tokyo, Japan
[2]Department of Radiology, Nippon Medical School Tama Nagayama Hospital, Tokyo, Japan

Background: We retrospectively examined image quality (IQ) of thin-slice virtual monochromatic imaging (VMI) of half-iodine-load, abdominopelvic, contrast-enhanced CT (CECT) by dual-energy CT (DECT) with deep learning image reconstruction (DLIR).

Methods: In 28 oncology patients with moderate-to-severe renal impairment undergoing half-iodine-load (300 mgI/kg) CECT by DECT during the nephrographic phase, we reconstructed VMI at 40-70 keV with a slice thickness of 0.625 mm using filtered back-projection (FBP), hybrid iterative reconstruction (HIR), and DLIR; measured contrast-noise ratio (CNR) of the liver, spleen, aorta, portal vein, and prostate/uterus; and determined the optimal keV to achieve the maximal CNR. At the optimal keV, two independent radiologists compared each organ's CNR and subjective IQ scores among FBP, HIR, and DLIR to subjectively grade image noise, contrast, sharpness, delineation of small structures, and overall IQ.

Results: CNR of each organ increased continuously from 70 to 40 keV using FBP, HIR, and DLIR. At 40 keV, CNR of the prostate/uterus was significantly higher with DLIR than with FBP; however, CNR was similar between FBP and HIR and between HIR and DLIR. The CNR of all other organs increased significantly from FBP to HIR to DLIR ($P < 0.05$). All IQ scores significantly improved from FBP to HIR to DLIR ($P < 0.05$) and were acceptable in all patients with DLIR only.

Conclusions: The combination of 40 keV and DLIR offers the maximal CNR and a subjectively acceptable IQ for thin-slice VMI of half-iodine-load CECT. (J Nippon Med Sch 2025; 92: 69–79)

Key words: deep learning image reconstruction, dual-energy CT, image quality, iodine load reduction, virtual monochromatic imaging

Introduction

Abdominopelvic contrast-enhanced computed tomography (CECT) is widely performed and requires sufficiently high spatial and contrast resolution, particularly for oncologic follow-up. Reducing slice thickness may improve diagnosis of fine recurrent, disseminated, and metastatic lesions, as well as diagnostic confidence, and decrease variability of tumor size measurement, leading to optimal patient management by decreasing partial-volume averaging and increasing spatial resolution[1–8]. However, image noise linearly increases because of the lower photon counts[9,10]. Achieving adequate contrast enhancement of the parenchymal organs requires a relatively large iodine load, which may increase the risk of contrast-induced nephropathy (CIN)[11]. A meta-analysis revealed associations between CIN and renal insufficiency, malignancy, and old age[12]; thus, iodine load in CECT examinations should be reduced, particularly for oncologic

† contributed equally; * co-correspondence
Correspondence to Toshiya Kariyasu, MD, PhD, Department of Radiology, Tokyo Women's Medical University Adachi Medical Center, 4–33–1 Kohoku, Adachi-ku, Tokyo 123–8558, Japan
E-mail: kariyasu.toshiya@twmu.ac.jp
https://doi.org/10.1272/jnms.JNMS.2025_92-112
Journal Website (https://www.nms.ac.jp/sh/jnms/)

follow-up in patients with renal insufficiency.

Dual-energy CT (DECT) uses two different X-ray spectra to simultaneously or near-simultaneously acquire two distinct datasets[13] and reconstruct various material- or energy-specific datasets, including virtual monochromatic imaging (VMI) at various energy levels (e.g., 40-140 keV)[14–16]. VMI depicts how the imaged object would look if the X-ray source produced only X-ray photons at a single energy. VMI at 40 keV, the closest to the K-edge of iodine (33.2 keV), can maximize iodine attenuation and reduce the iodine load while preserving contrast enhancement but, because of the lower photon counts, may maximize image noise and reduce lesion conspicuity[17,18]. Thus, reducing iodine load for VMI of a thin slice at 40 keV, which produces the most image noise and the lowest signal-noise ratio (SNR) and contrast-noise ratio (CNR)[19], appears challenging in abdominopelvic CECT because it frequently results in non-diagnostic image quality (IQ).

IQ has been improving since the recent introduction of deep learning image reconstruction (DLIR), which uses high-quality image data acquired at a high radiation dose that is further reconstructed with filtered back-projection (FBP) as targeting data[20,21]. There is a trade-off between spatial resolution and image noise in traditional filtered back-projection (FBP) and hybrid iterative reconstruction (HIR), which is currently the most popular algorithm in clinical CT examinations[22]. In contrast, previous phantom and clinical studies have reported that DLIR preserves spatial resolution with lower image noise than HIR[23,24]. It is uncertain, however, whether thin-slice VMI can preserve diagnostic IQ aided by DLIR in half-iodine-load CECT; further, the energy level that should be selected is unknown. Thus, this clinical pilot study retrospectively assessed the IQ of VMI at various energy levels of half-iodine-load abdominopelvic CECT of a thin slice reconstructed with FBP, HIR, and DLIR for oncologic follow-up of patients with renal insufficiency.

Materials and Methods

This retrospective study was approved by the relevant institutional review board (approval number: 2022-0104) and was conducted according to the principles of the Declaration of Helsinki.

Patients

We retrospectively enrolled 32 consecutive adult patients with malignancies and moderate-to-severe renal impairment (i.e., estimated glomerular filtration rate: <45 mL/min/1.73 m^2) who underwent half-iodine-load (300 mg iodine/kg) abdominopelvic CECT for oncologic follow-up using a 256-detector DECT scanner (Revolution CT; GE Healthcare, Milwaukee, Wis) as our routine clinical protocol, which was used whenever clinically applicable, between October 2021 and December 2021. The exclusion criteria were severe metallic/beam-hardening artifact(s) and difficulty in appropriate placement of regions of interest (ROIs) in the target organ(s), which precluded the IQ assessment described below. Four patients were excluded for a severe metallic artifact from a lumbar prosthesis (n = 1), severe beam-hardening artifact due to arms-down positioning (n = 1), difficulty in appropriate ROI placement (n = 2) due to a huge liver cyst (n = 1), and severe atrophy of the left hepatic lobe (n = 1). Thus, we ultimately included 28 patients [14 men, 14 women; mean age, 70 ± 10 years (45-88 years); mean body weight (BW), 62.1 ± 13.2 kg (41-97 kg); and mean body mass index (BMI), 23.8 ± 3.3 kg/m^2 (17-32 kg/m^2)] in this study (**Table 1**). No unexpected events, including technical failure, unstable breath-holding, or allergic reactions to contrast media (CM), were observed in any patient.

Table 1 Patient characteristics

Number of patients	28
Age (years) *	70 ± 10
Male/Female	14/14
Weight (kg) *	62.1 ± 13.2
BMI (kg/m^2) *	23.8 ± 3.3
Purpose of Examination	Oncologic follow-up
Primary Tumor	Renal cell carcinoma (20 cases), Prostatic cancer (3 cases), Bladder cancer (2 cases), Hepatocellular carcinoma (2 cases), Gastric cancer (1 case)

*Data are expressed as mean ± SD.
BMI, body mass index.

CT Image Acquisition and Reconstruction

The patients underwent helical abdominopelvic CECT acquisition with the DECT scanner using the following parameters: tube voltage, 80 and 140 kVp; tube current, 320-480 mA; rotation time, 0.6 s; pitch, 0.992:1; field of view, 32-40 cm; and detector collimation, 0.625 × 128 mm. All patients received non-ionic iodinated CM (Iopamiron 300; Bayer HealthCare, Osaka, Japan) at a concentration of 300 mg/mL. We administered 300 mg iodine/kg over 30 s via the right antecubital vein using a 22-gauge plastic intravenous catheter with a power injector (Dual Shot-type GX 7; Nemoto Kyorindo, Tokyo, Japan), and we began scanning after 100 s of CM administration. We reviewed the volume CT dose index ($CTDI_{vol}$) and dose-length product (DLP) recorded as a dose report to determine radiation exposure. We calculated the effective dose as the DLP multiplied by a k factor for the abdomen and pelvis of 0.015 $mSv \cdot mGy^{-1} \cdot cm^{-1}$ [25] for each patient. Thus, we calculated the mean $CTDI_{vol}$ and DLP and estimated the effective dose for this protocol. We equally calculated mean size-specific dose estimates (SSDE) to account for individual patient body habitus, as previously described[26]. For each patient, we reconstructed the VMI of the CECT at 40-70 keV (1-keV interval) with FBP, HIR (ASiR-V 40%, GE Healthcare), and DLIR (TrueFidelity Image-Medium, GE Healthcare) algorithms using the following parameters: matrix size, 512 × 512; minimal slice thickness, 0.625 mm; and field of view, 32-40 cm. We did not reconstruct the VMI at 71 keV or higher, which offers lower image contrast than single-energy CT (SECT) at 120 kVp, because the CT value of VMI at approximately 70 keV was reported to be equal to that of SECT at 120 kVp[19].

Quantitative IQ Assessment

On the axial VMI at 40-70 keV in each patient reconstructed by FBP, HIR, and DLIR and displayed on a commercially available workstation (Advantage Window Version 4.7, GE Healthcare), three radiology technologists (H.S., S.W., and F.R.) placed circular ROIs (area: 144.3 ± 125.9 mm^2) in the liver, spleen, abdominal aorta, portal vein, paraspinal muscle, and subcutaneous fat of the anterior abdominal wall in three consecutive slices at the level of the hepatic hilum, the prostate in men or uterus in women, the gluteus maximus muscle, and subcutaneous fat of the anterior abdominal wall in three consecutive slices at the level of the prostate/uterus. Then they measured the mean CT value of each anatomic structure and the standard deviation (SD) of the CT value. During the procedure, they carefully avoided any areas of focal changes in attenuation, prominent artifacts and large blood vessels in the parenchymal organs, and any macroscopically fatty area in the muscles. The CNR of each organ was calculated as the mean CT value of each organ minus that of the muscle divided by the SD of the CT value of fat in the abdomen and pelvis. The mean CNR of each organ was calculated at each keV to determine the optimal keV for achieving the maximum CNR of each organ.

Qualitative IQ Assessment

At a workstation, two independent board-certified radiologists (N.M. and K.T.)—who had 10 and 11 years of clinical experience, respectively, and were blinded to patient demographics and CT parameters—used a 4-point scale on a fixed window setting (window width, 650 HU; window level, 50 HU) to subjectively evaluate image noise, contrast, sharpness, delineation of small structures, and overall IQ of the VMI at the optimal keV reconstructed by FBP, HIR, and DLIR. Four points indicated excellent IQ, three points indicated good IQ, two points indicated fair IQ, and one point indicated poor IQ. Here, two to four points were considered diagnostic and one point as non-diagnostic.

Statistical Analysis

All continuous variables were expressed as mean ± SD, and all categorical variables were expressed as median (interquartile range [IQR]). Commercially available statistical software SPSS for Windows, Version 23.0 (IBM SPSS, Armonk, NY, USA) was used to perform statistical analysis. The Kruskal-Wallis test with Bonferroni correction was used to compare each organ's CT value, CNR, and subjective IQ scores on the VMI at the optimal keV among FBP, HIR, and DLIR. The weighted kappa test was used to estimate inter-reviewer agreement. $P < 0.05$ was considered to be statistically significant.

Our institutional review board approved this retrospective study, and all patients provided written informed consent.

Results

The mean $CTDI_{vol}$ was 14.3 ± 0.8 mGy; DLP, 1,074.5 ± 104.5 mGy · cm; estimated effective dose, 16.1 ± 1.6 mSv; and SSDE, 18.0 ± 1.4 mGy.

Quantitative IQ Assessment

The CT value and CNR of every organ increased continuously from 70 keV to 40 keV with FBP, HIR, and DLIR (**Fig. 1, 2**). Thus, the optimal keV for all organs using all three reconstruction algorithms was 40 keV. At the optimal keV, CT values of all organs were comparable among FBP, HIR, and DLIR (P = 0.89-1.00) (**Table 2**); however, CNR of the prostate/uterus was significantly greater with DLIR than with FBP (P = 0.01) but comparable between FBP and HIR (P = 0.53) and between HIR and DLIR (P = 0.08). CNR of any other organs increased significantly from FBP to HIR to DLIR (P < 0.01 for all) (**Table 3**).

Qualitative IQ Assessment

All IQ scores at the optimal keV (i.e., 40 keV) improved significantly from FBP to HIR to DLIR (P < 0.001 for all) and were acceptable in 17/28 patients (61%) with FBP, 27/28 patients (96%) with HIR, and all patients with DLIR (**Table 4** and **Fig. 3**). Inter-reviewer agreement was

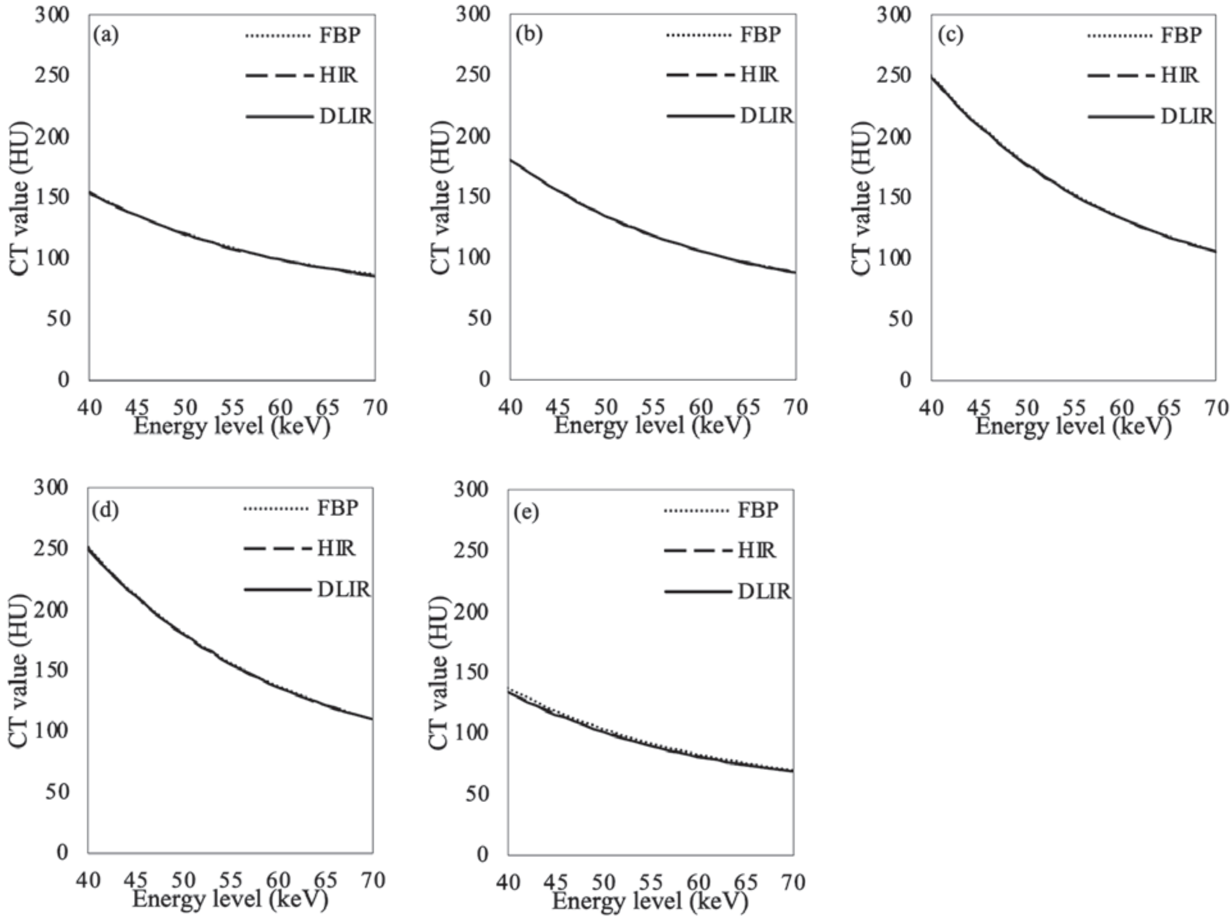

Fig. 1 Line graphs of the CT value of the liver (**a**), spleen (**b**), aorta (**c**), portal vein (**d**), and prostate/uterus (**e**) on VMI at 40–70 keV reconstructed with FBP, HIR, and DLIR. The CT values for all organs increased continuously from 70 to 40 keV with FBP, HIR, and DLIR.
CT, computed tomography; DLIR, deep learning image reconstruction; FBP, filtered back projection; HIR, hybrid iterative reconstruction; VMI, virtual monochromatic imaging.

substantial (κ = 0.65).

As shown in representative cases (**Fig. 4, 5**), on VMI at 40 keV of half-iodine-load, abdominopelvic CECT with minimal slice thickness, low-contrast lesions, such as liver metastases (**Fig. 4**) and a mass protruding into the bladder (**Fig. 5**), are better delineated mainly because there was less image noise from FBP to HIR to DLIR. In particular, with DLIR, IQ, including natural image noise and texture, appears well preserved even with minimal slice thickness, which allows generation of high-quality multiplanar reformation (MPR) images. Specifically, overall IQ was graded as 1 and 2 for FBP, 2 and 3 for HIR, and 4 and 4 for DLIR by reviewers 1 and 2, respectively, in the former patient (**Fig. 4**), and 2 and 2 for FBP, 3 and 2 for HIR, and 4 and 4 for DLIR in the latter patient (**Fig. 5**).

Discussion

In this study, focusing on the VMI of half-iodine-load abdominopelvic CECT with 0.625-mm slice thickness for oncologic follow-up in patients with moderate-to-severe renal impairment, the CT value and CNR increased continuously from 70 to 40 keV; thus, 40 keV was the optimal keV to achieve the maximum CNR, which was obtained with FBP, HIR, and DLIR in all organs.

To our knowledge, this is a novel finding obtained by detailed quantitative comparison of the CNR at 40-70 keV (1-keV interval), whereas an intermediate energy range of approximately 60-70 keV has been so far reported to maximize CNR[18,27,28]. This may be attributable to our advanced DECT hardware, which is equipped with gemstone detectors that offer approximately 2.5 times more views with 1,000 times faster primary speed and four times less afterglow than standard CT systems. The present DECT system uses a fast tube voltage switching technique that synchronously optimizes tube current or photon flux between the low and high tube voltages (i.e., 80 and 140 kVp), unlike the conventional technique,

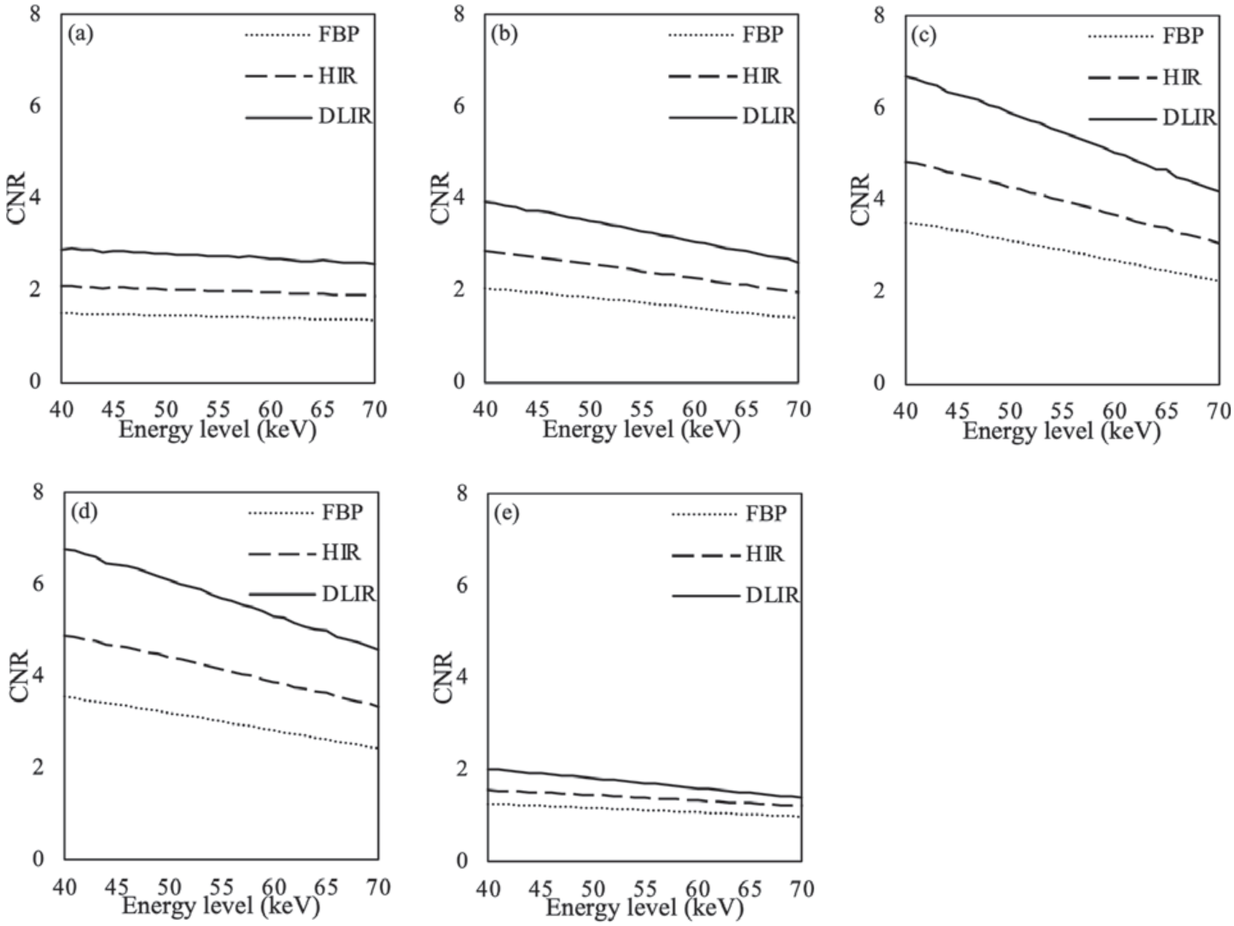

Fig. 2 Line graphs of the CNR of the liver (**a**), spleen (**b**), aorta (**c**), portal vein (**d**), and prostate/uterus (**e**) on VMI at 40–70 keV reconstructed with FBP, HIR, and DLIR. CNR values for all organs increased continuously from 70 to 40 keV with FBP, HIR, and DLIR.
CNR, contrast-noise ratio; DLIR, deep learning image reconstruction; FBP, filtered back projection; HIR, hybrid iterative reconstruction; VMI, virtual monochromatic imaging.

Table 2 CT values at 40 keV

	FBP	HIR	DLIR	*P* value
Liver	154.3 ± 23.7	153.7 ± 24.1	154.0 ± 23.8	0.99
Spleen	181.1 ± 15.7	181.0 ± 14.4	180.7 ± 14.7	0.99
Aorta	250.1 ± 25.6	248.7 ± 24.8	249.1 ± 24.7	0.97
Portal vein	251.0 ± 30.0	249.7 ± 28.9	250.1 ± 29.4	1.00
Prostate/Uterus	137.5 ± 35.8	134.2 ± 35.6	133.9 ± 37.1	0.89

Data are expressed as mean ± SD (in HU).
CT, computed tomography; DLIR, deep learning image reconstruction; FBP, filtered back projection; HIR, hybrid iterative reconstruction.

which exposes a constant tube current or photon flux between the two different tube voltages[29]. As compared with the conventional fast tube voltage switching technique that exposes a constant tube current (mA), improving a low-kVp signal with this synchronized kVp and mA switching technique is particularly beneficial for improving IQ of VMI at a low energy level.

At 40 keV, the CNR of the prostate/uterus was significantly higher with DLIR than with FBP but comparable between FBP and HIR and between HIR and DLIR. The CNR of all other organs increased significantly from FBP to HIR to DLIR. All qualitative IQ scores at 40 keV significantly improved from FBP to HIR to DLIR and were acceptable in all patients with DLIR only. Our CT acquisition protocol exposed radiation doses comparable to or lower than the diagnostic reference levels for low-dose

Table 3 CNR at 40 keV

	FBP	HIR	DLIR	*P* value	*P* value (FBP vs. HIR)	*P* value (FBP vs. DLIR)	*P* value (HIR vs. DLIR)
Liver	1.5 ± 0.6	2.1 ± 0.8	2.9 ± 1.1	<0.001	0.003	<0.001	0.002
Spleen	2.0 ± 0.5	2.9 ± 0.7	3.9 ± 0.9	<0.001	<0.001	<0.001	<0.001
Aorta	3.5 ± 0.8	4.8 ± 1.0	6.7 ± 1.4	<0.001	<0.001	<0.001	<0.001
Portal vein	3.5 ± 0.9	4.9 ± 1.2	6.8 ± 1.8	<0.001	<0.001	<0.001	<0.001
Prostate/Uterus	1.2 ± 1.3	1.5 ± 1.7	2.0 ± 1.5	0.04	0.53	0.01	0.08

Data are expressed as mean ± SD.
CNR, contrast-noise ratio; DLIR, deep learning image reconstruction; FBP, filtered back projection; HIR, hybrid iterative reconstruction.

Table 4 Qualitative IQ scores at 40 keV

	FBP	HIR	DLIR	*P* value	*P* value (FBP vs. HIR)	*P* value (FBP vs. DLIR)	*P* value (HIR vs. DLIR)
Image noise	2.0 (2.0-2.0)	3.0 (2.5-3.0)	4.0 (3.5-4.0)	<0.001	<0.001	<0.001	<0.001
Image contrast	2.0 (2.0-2.0)	3.0 (2.9-3.0)	4.0 (3.5-4.0)	<0.001	<0.001	<0.001	<0.001
Sharpness	2.0 (2.0-2.0)	3.0 (2.5-3.0)	4.0 (4.0-4.0)	<0.001	<0.001	<0.001	<0.001
Small-structure delineation	2.0 (1.5-2.0)	3.0 (2.5-3.0)	4.0 (3.5-4.0)	<0.001	<0.001	<0.001	<0.001
Overall IQ	2.0 (2.0-2.0)	3.0 (2.9-3.0)	4.0 (4.0-4.0)	<0.001	<0.001	<0.001	<0.001

Data are expressed as median (inter-quartile range).
DLIR, deep learning image reconstruction; FBP, filtered back projection; HIR, hybrid iterative reconstruction; IQ, image quality.

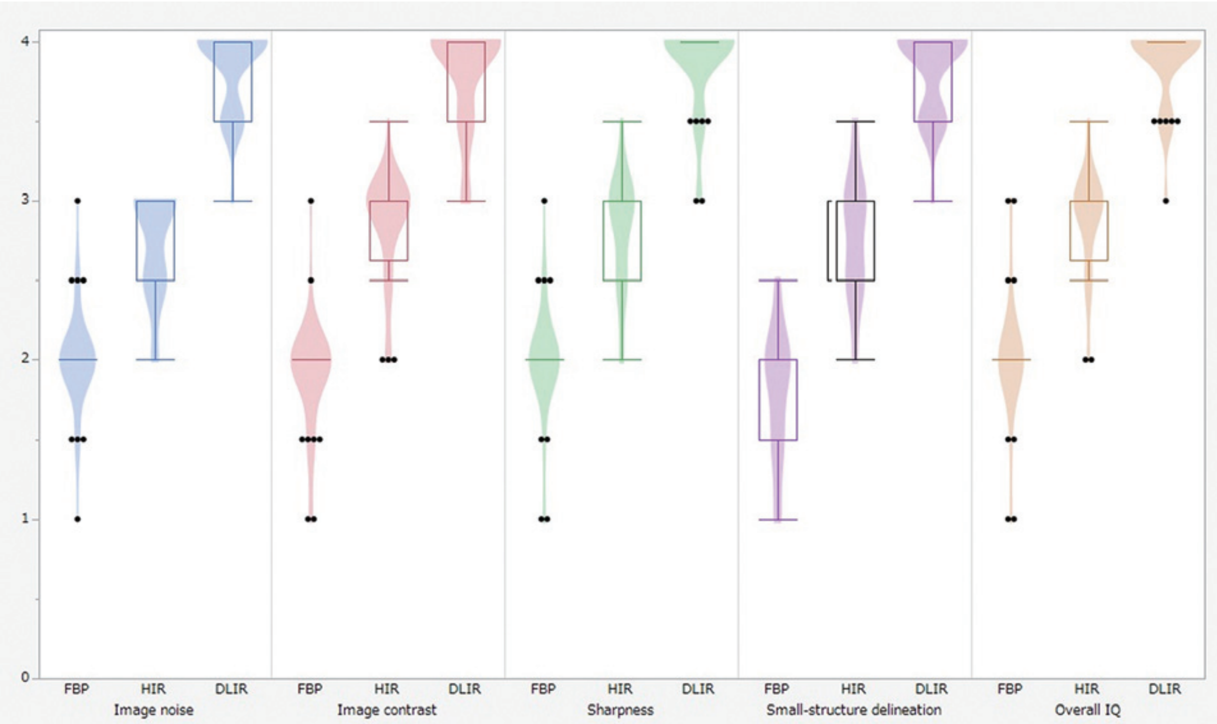

Fig. 3 Violin plots with box-and-whisker plots representing the qualitative IQ scores on VMI at 40 keV reconstructed with FBP, HIR, and DLIR. All IQ scores significantly improved from FBP to HIR to DLIR ($P < 0.001$ for all).
DLIR, deep learning image reconstruction; FBP, filtered back projection; HIR, hybrid iterative reconstruction; IQ, image quality; VMI, virtual monochromatic imaging.

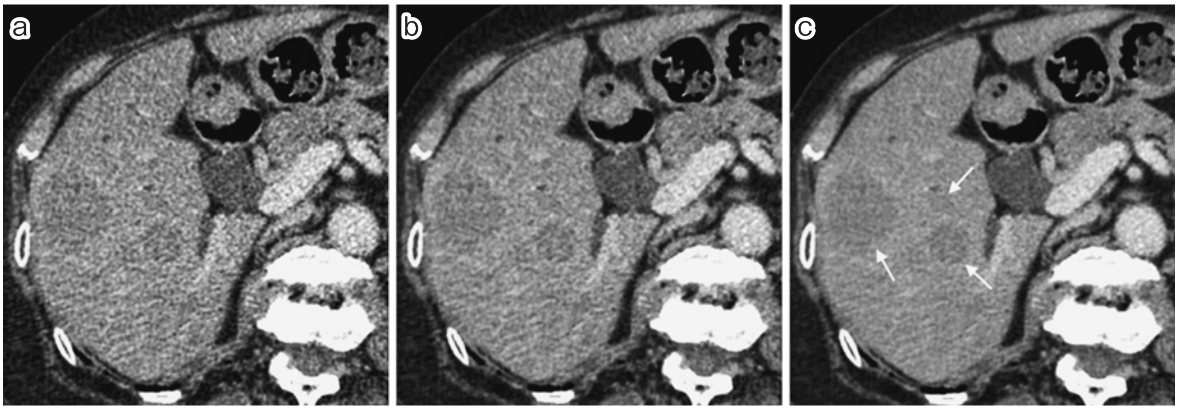

Fig. 4 Axial images (**a-c**) of VMI at 40 keV of contrast-enhanced CT of the abdomen with 0.625-mm slice thickness reconstructed with FBP (**a**), HIR (**b**), and DLIR (**c**) in a 72-year-old woman (144 cm, 47 kg, body mass index [BMI]: 22.6 kg/m^2) with liver metastases (arrows). These low-contrast hepatic masses are better delineated with less image noise from FBP (**a**) to HIR (**b**) to DLIR (**c**). In particular, with DLIR (**c**), IQ, including natural image noise and texture, appears well preserved even with this slice thickness.
CT, computed tomography; DLIR, deep learning image reconstruction; FBP, filtered back projection; HIR, hybrid iterative reconstruction; IQ, image quality; VMI, virtual monochromatic imaging.

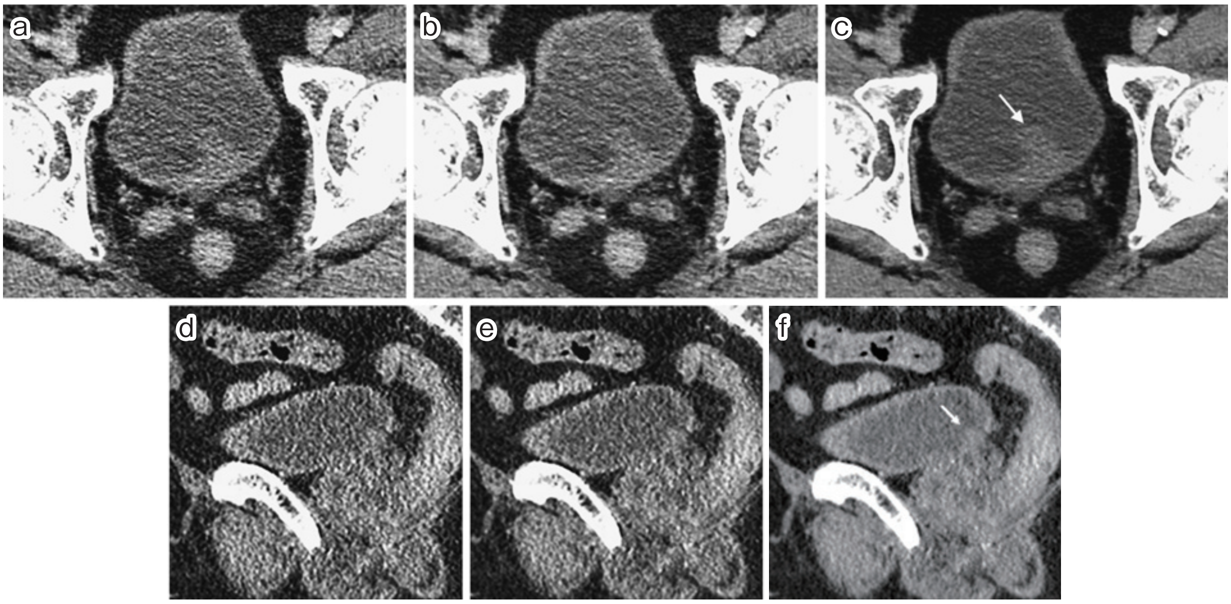

Fig. 5 Axial (**a-c**) and MPR sagittal images (**d-f**) of VMI at 40 keV of contrast-enhanced CT of the pelvis with 0.625-mm slice thickness reconstructed with FBP (**a**, **d**), HIR (**b**, **e**), and DLIR (**c**, **f**) in an 80-year-old man (173 cm, 81 kg, body mass index [BMI]: 27.1 kg/m^2) with a mass protruding into the bladder (arrow). The low contrast mass is better delineated with less image noise from FBP (**a**, **d**) to HIR (**b**, **e**) to DLIR (**c**, **f**). In particular, with DLIR (**c**, **f**), IQ, including natural image noise and texture, appears well preserved even with this slice thickness.
CT, computed tomography; DLIR, deep learning image reconstruction; FBP, filtered back projection; HIR, hybrid iterative reconstruction; IQ, image quality; MPR, multiplanar reformation; VMI, virtual monochromatic imaging.

abdominopelvic CT that are used in many countries ($CTDI_{vol}$: 13-18 mGy)[30,31]. Thus, to our knowledge, this is the first study to demonstrate the clinical acceptability of VMI at 40 keV of half-iodine-load abdominopelvic CECT of the thin slice aided by DLIR for oncologic follow-up.

Several studies have demonstrated the superior performance in IQ and lesion detection of DLIR algorithms, which are currently available from multiple vendors, to FBP and HIR algorithms[2,25,32-41]. Our DLIR algorithm uses high-quality image data acquired at a high radiation dose and then performs reconstruction with FBP as targeting data[20,21]. Thus, our algorithm significantly reduces image noise, as compared with FBP and HIR[21,25,42,43], and better preserves the FBP-like natural noise texture, resulting in a sharper image than HIR[25,43]. The DLIR can provide better IQ clinically with less coarseness of image texture and better subjective acceptance by radiologists because of the reduced low-frequency noise[2,44,45]. It was also found to improve low-contrast lesion detectability and reduce radiation dose, as compared with HIR[25,29,43].

Use of the thin slice in the CECT can maximally decrease partial-volume averaging and increase spatial resolution, thus improving diagnosis of fine, recurrent, disseminated, and metastatic lesions. It also improves diagnostic confidence and decreases variability of tumor size measurement for oncologic follow-up, leading to optimal patient management, also by reducing pseudoenhancement and generating excellent isotropic MPR images and other three-dimensional reconstruction (e.g., maximum intensity projection and volume rendering) images[1–7]. In Japan, a clinical practice guideline for gastrointestinal stromal tumors recommends, when applicable, the acquisition of volume data at a slice thickness of 2 mm or thinner by multi-detector CT[46]. Use of 1-mm slice and MPR images was reported to improve sensitivity and diagnostic confidence of peritoneal carcinomatosis[6]. In addition, radiomics is being increasingly used to mechanically extract quantifiable image features, thereby aiding in diagnosis and prognosis prediction. Thin-slice images are preferred for extracting these quantitative features with high reproducibility; however, the increased noise inherent in thin-slice images may affect the accuracy of texture features. Therefore, balancing slice thickness and noise reduction is crucial for optimizing feature extraction and ensuring reliable radiomics analysis outcomes[47–50]. Although use of thinner slices with better spatial resolution enables detection of more lesions, lower SNR can impair characterization of low-contrast lesions such as small metastases[8,51]. In SECT with a 1.25-mm slice thickness, DLIR significantly reduced image noise in the detection of low-contrast lesions, as compared with HIR, while also substantially improving spatial resolution and overall IQ[52]. In VMI at 74 keV of abdominal CECT with a slice thickness of 2.5 mm and 0.625 mm, DLIR improved image noise levels, as compared with HIR[53]. VMI at 70 keV with DLIR in low-dose images with a 1.25-mm slice thickness demonstrated comparable image noise, SNR, and CNR to standard-dose images with a 5-mm slice thickness using HIR[54].

According to a meta-analysis, iodine load in CECT examinations should be limited to a reasonable amount to reduce the risk of CIN, especially for oncologic follow-up in patients with renal insufficiency[12]. VMI at 40 keV, closest to the K-edge of iodine, can maximize iodine attenuation and decrease iodine load while maintaining contrast enhancement. However, VMI at a low energy level is subjected to more noise and may not be ideal for every diagnostic task[18]. VMI at 40 keV using DLIR significantly reduced image noise, as compared with HIR, and substantially improved IQ, especially in thin-slice images, based on subjective evaluations[53]. VMI at 40 keV using DLIR exhibited a noise texture comparable to SECT at 120 kVp using HIR, while improving SNR and lesion conspicuity and providing equal or superior subjective IQ[55]. Further, in body CECT with a 5-mm slice thickness, VMI at 40 keV aided by DLIR was reported to allow a half-iodine load while maintaining diagnostic IQ[21]. Unlike the present study, that previous study did not use thin-slice images or determine the optimal keV by detailed quantitative CNR comparison; that is, it is uncertain why 40 keV was selected. Noda et al.[56] reported the clinical acceptability of combined use of thin-slice VMI at 40 keV and DLIR for half-iodine-load CT angiography, in which high-contrast structures of interest are primarily evaluated. In contrast, we are the first to demonstrate the clinical acceptability of this combination for assessment of low-contrast solid organs in half-iodine-load abdominopelvic CECT.

The reason why the CNR in the pelvis was similar between HIR and DLIR in our study is possibly the current unavailability of an automatic tube current modulation program for our DECT scanner. This program, in which the tube current is automatically adjusted in relation to the patient's body size to optimize the radiation dose and maintain image noise, is equipped only for SECT. Thus, insufficient radiation exposure might not significantly decrease the image noise in the VMI of the pelvic region using DLIR[56]. A modulation program may be introduced for DECT to further improve IQ on VMI of the pelvic region with DLIR and substantially reduce radiation dose in the future. On the other hand, qualitative IQ, including that of the pelvic region, was significantly higher with DLIR than with HIR, and diagnostic IQ was more frequently achieved with DLIR than with HIR in this study.

The limitations of our study are as follows. First, it included only a small study population at a single institution, and our findings might have been affected by the BW and BMI of our Japanese patients, which were lower than those of average-sized patients in Western countries. Second, as part of our routine oncologic follow-up examinations, we acquired CECT only during the nephrographic phase. IQ depends more on total iodine dose during this phase than during the arterial phase, and image contrast is generally greater, resulting in more sensitive detection of fine recurrent, disseminated, and metastatic lesions during this phase than during the delayed phase. Third, we used a minimum slice thickness of 0.625 mm only and did not use other slice thicknesses. Increased slice thicknesses can reduce image noise and improve IQ, which might reduce the superiority of DLIR to FBP and HIR, as demonstrated in our study. In addition, we did not compare IQ between the thin slice and 5-mm slice. Finally, we assessed only IQ in CECT and did not examine lesion delineation or diagnostic performance. To confirm the present clinical benefits, future studies should examine lesion delineation and diagnostic performance in a larger cohort at multiple institutions.

Conclusions

The combination of 40 keV and DLIR provides the maximum CNR and a subjectively acceptable IQ in thin-slice VMI of half-iodine-load abdominopelvic CECT for oncologic follow-up in patients with moderate-to-severe renal impairment. This combination may improve diagnosis of fine recurrent, disseminated, and metastatic lesions, increase diagnostic confidence, and decrease the variability of tumor size measurement, leading to optimal patient management while reducing the risk of CIN.

Conflict of Interest: None declared.

References

1. Hamabe F, Mikoshi A, Edo H, et al. Effect of ultra-high-resolution CT on pseudoenhancement in renal cysts: A phantom experiment and clinical study. AJR Am J Roentgenol [Internet]. 2022 Oct;219(4):624–33. Epub 2022 May 18. Available from: https://www.ajronline.org/doi/10.2214/AJR.22.27354. doi: 10.2214/AJR.22.27354. Erratum in: AJR Am J Roentgenol. 2022 Dec;219(6):1012. doi: 10.2214/AJR.22.28586. PubMed PMID: 35583427
2. Nishikawa M, Machida H, Shimizu Y, et al. Image quality and radiologists' subjective acceptance using model-based iterative and deep learning reconstructions as adjuncts to ultrahigh-resolution CT in low-dose contrast-enhanced abdominopelvic CT: Phantom and clinical pilot studies. Abdom Radiol [Internet]. 2022 Feb;47(2):891–902. Epub 2021 Dec 16. Available from: https://link.springer.com/article/10.1007/s00261-021-03373-5. doi: 10.1007/s00261-021-03373-5. PubMed PMID: 34914007; PubMed Central PMCID: PMC8807451
3. Raman SP, Fishman EK. Advances in CT imaging of GI malignancies. Gastrointest Cancer Res [Internet]. 2012 May;5(3 Suppl 1):S4–9. Available from: https://pmc.ncbi.nlm.nih.gov/articles/PMC3413036. PubMed PMID: 22876336; PubMed Central PMCID: PMC3413036
4. Heckel F, Meine H, Moltz JH, et al. Segmentation-based partial volume correction for volume estimation of solid lesions in CT. IEEE Trans Med Imaging [Internet]. 2014 Feb;33(2):462–80. Epub 2013 Oct 28. Available from: https://ieeexplore.ieee.org/document/6648691. doi: 10.1109/TMI.2013.2287374. PubMed PMID: 24184707
5. Fabel M, Wulff A, Heckel F, et al. Clinical lymph node staging--Influence of slice thickness and reconstruction kernel on volumetry and RECIST measurements. Eur J Radiol [Internet]. 2012 Nov;81(11):3124–30. Epub 2012 Mar 29. Available from: https://www.sciencedirect.com/science/article/pii/S0720048X12001039?via%3Dihub. doi: 10.1016/j.ejrad.2012.03.008. PubMed PMID: 22464844
6. Franiel T, Diederichs G, Engelken F, Elgeti T, Rost J, Rogalla P. Multi-detector CT in peritoneal carcinomatosis: Diagnostic role of thin slices and multiplanar reconstructions. Abdom Imaging [Internet]. 2009 Jan-Feb;34(1):49–54. Available from: https://link.springer.com/article/10.1007/s00261-008-9372-z. doi: 10.1007/s00261-008-9372-z. PubMed PMID: 18264738
7. Sandrasegaran K, Rydberg J, Akisik F, Hameed TA, Dunkle JW. Isotropic CT examination of abdomen and pelvis: Diagnostic quality of reformat. Acad Radiol [Internet]. 2006 Nov;13(11):1338–43. Available from: https://www.sciencedirect.com/science/article/abs/pii/S1076633206004156?via%3Dihub. doi: 10.1016/j.acra.2006.04.019. PubMed PMID: 17070451
8. Smith JT, Hawkins RM, Guthrie JA, et al. Effect of slice thickness on liver lesion detection and characterisation by multidetector CT. J Med Imaging Radiat Oncol. 2010 Jun;54(3):188–93. doi: 10.1111/j.1754-9485.2010.02157.x. PubMed PMID: 20598005
9. Ford JM, Decker SJ. Computed tomography slice thickness and its effects on three-dimensional reconstruction of anatomical structures. J Forensic Radiol Imaging. 2016;4:43–6. doi: 10.1016/j.jofri.2015.10.004
10. Manson EN, Fletcher JJ, Amuasi JH. Variation of noise with some scanning parameters for image quality test in 128 slice computed tomography scanner using Catphan 700 phantom. J Radiol Diagn Methods. 2018;1(1):102.
11. Gupta S, Motwani SS, Seitter RH, et al. Development and validation of a risk model for predicting contrast-associated acute kidney injury in patients with cancer: Evaluation in over 46,000 CT examinations. AJR Am J Roentgenol. 2023 Oct;221(4):486–501. Epub 2023 May 17. doi: 10.2214/AJR.23.29139. Erratum in: AJR Am J Roentgenol. 2023 Oct;221(4):561. doi: 10.2214/AJR.23.30129. PubMed PMID: 37195792
12. Moos SI, van Vemde DN, Stoker J, Bipat S. Contrast induced nephropathy in patients undergoing intravenous (IV) contrast enhanced computed tomography (CECT) and the relationship with risk factors: A meta-analysis. Eur J Radiol [Internet]. 2013 Sep;82(9):e387–99. Epub 2013 May 25. doi: 10.1016/j.ejrad.2013.04.029. PubMed PMID: 23711425
13. McCollough CH, Leng S, Yu L, Fletcher JG. Dual- and Multi-Energy CT: Principles, technical approaches, and clinical applications. Radiology. 2015 Sep;276(3):637–53. doi: 10.1148/radiol.2015142631. PubMed PMID: 26302388; PubMed Central PMCID: PMC4557396
14. Im AL, Lee YH, Bang DH, Yoon KH, Park SH. Dual energy CT in patients with acute abdomen; is it possible for virtual non-enhanced images to replace true non-enhanced images? Emerg Radiol. 2013 Dec;20(6):475–83. Epub 2013 Jul 3. doi: 10.1007/s10140-013-1141-9. PubMed PMID: 23821015
15. Ascenti G, Mileto A, Gaeta M, Blandino A, Mazziotti S,

Scribano E. Single-phase dual-energy CT urography in the evaluation of haematuria. Clin Radiol. 2013 Feb;68(2): e87–94. Epub 2012 Dec 6. doi: 10.1016/j.crad.2012.11.001. PubMed PMID: 23219453

16. Fornaro J, Leschka S, Hibbeln D, et al. Dual- and multi-energy CT: approach to functional imaging. Insights Imaging. 2011 Apr;2(2):149–59. Epub 2011 Jan 19. doi: 10.1007/s13244-010-0057-0. PubMed PMID: 22347944; PubMed Central PMCID: PMC3259372
17. Albrecht MH, Vogl TJ, Martin SS, et al. Review of clinical applications for virtual monoenergetic dual-energy CT. Radiology. 2019 Nov;293(2):260–71. Epub 2019 Sep 10. doi: 10.1148/radiol.2019182297. PubMed PMID: 31502938
18. D'Angelo T, Cicero G, Mazziotti S, et al. Dual energy computed tomography virtual monoenergetic imaging: technique and clinical applications. Br J Radiol. 2019 Jun; 92(1098):20180546. Epub 2019 Apr 9. doi: 10.1259/bjr.20180546. PubMed PMID: 30919651; PubMed Central PMCID: PMC6592074
19. Matsumoto K, Jinzaki M, Tanami Y, Ueno A, Yamada M, Kuribayashi S. Virtual monochromatic spectral imaging with fast kilovoltage switching: Improved image quality as compared with that obtained with conventional 120-kVp CT. Radiology [Internet]. 2011 Apr;259(1):257–62. Epub 2011 Feb 17. doi: 10.1148/radiol.11100978. PubMed PMID: 21330561
20. Noda Y, Kawai N, Nagata S, et al. Deep learning image reconstruction algorithm for pancreatic protocol dual-energy computed tomography: Image quality and quantification of iodine concentration. Eur Radiol [Internet]. 2022 Jan;32(1):384–94. Epub 2021 Jun 15. doi: 10.1007/s00330-021-08121-3. PubMed PMID: 34131785
21. Noda Y, Kawai N, Kawamura T, et al. Radiation and iodine dose reduced thoraco-abdomino-pelvic dual-energy CT at 40 keV reconstructed with deep learning image reconstruction. Br J Radiol [Internet]. 2022 Jun;95(1134): 20211163. PubMed PMID: 35230135
22. Mileto A, Guimaraes LS, McCollough CH, Fletcher JG, Yu L. State of the art in abdominal CT: The limits of iterative reconstruction algorithms. Radiology. 2019 Dec;293(3): 491–503. Epub 2019 Oct 29. doi: 10.1148/radiol.2019191422. PubMed PMID: 31660806
23. Nagayama Y, Goto M, Sakabe D, et al. Radiation dose optimization potential of deep learning-based reconstruction for multiphase hepatic CT: A clinical and phantom study. Eur J Radiol. 2022 Jun;151:110280. Epub 2022 Apr 1. doi: 10.1016/j.ejrad.2022.110280
24. Nagayama Y, Goto M, Sakabe D, et al. Radiation dose reduction for 80-kVp Pediatric CT using deep learning-based reconstruction: A clinical and phantom study. AJR Am J Roentgenol. 2022 Aug;219(2):315–24. Epub 2022 Feb 23. doi: 10.2214/AJR.21.27255. PubMed PMID: 35195431
25. Greffier J, Hamard A, Pereira F, et al. Image quality and dose reduction opportunity of deep learning image reconstruction algorithm for CT: A phantom study. Eur Radiol [Internet]. 2020 Jul;30(7):3951–9. Epub 2020 Feb 25. doi: 10.1007/s00330-020-06724-w. PubMed PMID: 32100091
26. Boone JM, Strauss KJ, Cody DD, et al. AAPM report 204: Size-specific dose estimates in pediatric and adult body CT examinations. Alexandria (VA): American Association of Physicists in Medicine; 2011 [Internet]. Available from: https://www.aapm.org/pubs/reports/rpt_204.pdf
27. Albrecht MH, Scholtz JE, Husers K, et al. Advanced image-based virtual monoenergetic dual-energy CT angiography of the abdomen: optimization of kiloelectron volt settings to improve image contrast. Eur Radiol. 2016 Jun; 26(6):1863–70. Epub 2015 Sep 3. doi: 10.1007/s00330-015-3970-2. PubMed PMID: 26334508
28. Apfaltrer P, Sudarski S, Schneider D, et al. Value of monoenergetic low-kV dual energy CT datasets for improved image quality of CT pulmonary angiography. Eur J Radiol. 2014 Feb;83(2):322–8. Epub 2013 Nov 23. doi: 10.1016/j.ejrad.2013.11.005. PubMed PMID: 24361061
29. Thibault JB, Utschig M. Revolution apex with quantix™ 160 - when power meets coverage. Chicago (IL): GE Healthcare; 2020 [Internet]. Available from: https://www.gehealthcare.com/-/jssmedia/global/products/images/revolution-apex-platform/quantix_whitepaper_jb78157xx.pdf?rev=-1
30. Tonkopi E, Duffy S, Abdolell M, Manos D. Diagnostic reference levels and monitoring practice can help reduce patient dose from CT examinations. AJR Am J Roentgenol. 2017 May;208(5):1073–81. Epub 2017 Feb 28. doi: 10.2214/AJR.16.16361. PubMed PMID: 28245142
31. Matsunaga Y, Chida K, Kondo Y, et al. Diagnostic reference levels and achievable doses for common computed tomography examinations: Results from the japanese nationwide dose survey. Br J Radiol [Internet]. 2019 Feb;92(1094):20180290. Epub 2018 Oct 24. Available from: https://pmc.ncbi.nlm.nih.gov/articles/PMC6404832. doi: 10.1259/bjr.20180290. PubMed PMID: 30306794; PubMed Central PMCID: PMC6404832
32. Xu JJ, Lonn L, Budtz-Jorgensen E, Hansen KL, Ulriksen PS. Quantitative and qualitative assessments of deep learning image reconstruction in low-keV virtual monoenergetic dual-energy CT. Eur Radiol. 2022 Oct;32(10):7098–107. Epub 2022 Jul 27. doi: 10.1007/s00330-022-09018-5. PubMed PMID: 35895120
33. Fukutomi A, Sofue K, Ueshima E, et al. Deep learning image reconstruction to improve accuracy of iodine quantification and image quality in dual-energy CT of the abdomen: a phantom and clinical study. Eur Radiol. 2023 Feb;33(2):1388–99. Epub 2022 Sep 17. doi: 10.1007/s00330-022-09127-1. PubMed PMID: 36114848
34. Nagata M, Ichikawa Y, Domae K, et al. Application of deep learning-based denoising technique for radiation dose reduction in dynamic abdominal CT: Comparison with standard-dose CT using hybrid iterative reconstruction method. J Digit Imaging. 2023 Aug;36(4):1578–87. Epub 2023 Mar 21. doi: 10.1007/s10278-023-00808-x. PubMed PMID: 36944812; PubMed Central PMCID: PMC10406991
35. Kawashima H, Ichikawa K, Takata T, et al. Performance of clinically available deep learning image reconstruction in computed tomography: a phantom study. J Med Imaging (Bellingham). 2020 Nov;7(6):063503. Epub 2020 Dec 16. doi: 10.1117/1.JMI.7.6.063503. PubMed PMID: 33344672; PubMed Central PMCID: PMC7739999
36. Park HJ, Choi SY, Lee JE, et al. Deep learning image reconstruction algorithm for abdominal multidetector CT at different tube voltages: assessment of image quality and radiation dose in a phantom study. Eur Radiol. 2022 Jun; 32(6):3974–84. Epub 2022 Jan 22. doi: 10.1007/s00330-021-08459-8. PubMed PMID: 35064803
37. Yoshida K, Nagayama Y, Funama Y, et al. Low tube voltage and deep-learning reconstruction for reducing radiation and contrast medium doses in thin-slice abdominal CT: a prospective clinical trial. Eur Radiol. 2024 Nov;34(11):7386–96. Epub 2024 May 16. doi: 10.1007/s00330-024-10793-6. PubMed PMID: 38753193
38. Cao L, Liu X, Li J, et al. A study of using a deep learning image reconstruction to improve the image quality of ex-

tremely low-dose contrast-enhanced abdominal CT for patients with hepatic lesions. Br J Radiol. 2021 Feb 1;94 (1118):20201086. Epub 2020 Dec 11. doi: 10.1259/bjr.20201086. PubMed PMID: 33242256; PubMed Central PMCID: PMC7934287

39. Kim JH, Yoon HJ, Lee E, Kim I, Cha YK, Bak SH. Validation of deep-learning image reconstruction for low-dose chest computed tomography scan: Emphasis on image quality and noise. Korean J Radiol. 2021 Jan;22(1):131–8. Epub 2020 Jul 27. doi: 10.3348/kjr.2020.0116. PubMed PMID: 32729277; PubMed Central PMCID: PMC7772377
40. Nakamura Y, Narita K, Higaki T, Akagi M, Honda Y, Awai K. Diagnostic value of deep learning reconstruction for radiation dose reduction at abdominal ultra-high-resolution CT. Eur Radiol. 2021 Jul;31(7):4700–9. Epub 2021 Jan 3. doi: 10.1007/s00330-020-07566-2. PubMed PMID: 33389036
41. Zhang X, Zhang G, Xu L, et al. Application of deep learning reconstruction of ultra-low-dose abdominal CT in the diagnosis of renal calculi. Insights Imaging. 2022 Oct 8;13 (1):163. doi: 10.1186/s13244-022-01300-w. PubMed PMID: 36209195; PubMed Central PMCID: PMC9547757
42. Benveniste AP, de Castro Faria S, Broering G, et al. Potential application of dual-energy CT in gynecologic cancer: Initial experience. Am J Roentgenol [Internet]. 2017 Mar; 208(3):695–705. Epub 2017 Jan 11. doi: 10.2214/AJR.16.16227. Erratum in: AJR Am J Roentgenol. 2017 May;208(5):1176. doi: 10.2214/AJR.17.18227. PubMed PMID: 28075606
43. Racine D, Brat HG, Dufour B, et al. Image texture, low contrast liver lesion detectability and impact on dose: Deep learning algorithm compared to partial model-based iterative reconstruction. Eur J Radiol [Internet]. 2021 Aug;141:109808. Epub 2021 Jun 3. doi: 10.1016/j.ejrad.2021.109808. PubMed PMID: 34120010
44. Laurent G, Villani N, Hossu G, et al. Full model-based iterative reconstruction (MBIR) in abdominal CT increases objective image quality, but decreases subjective acceptance. Eur Radiol [Internet]. 2019 Aug;29(8):4016–25. Epub 2019 Jan 30. doi: 10.1007/s00330-018-5988-8. PubMed PMID: 30701327
45. Higaki T, Nakamura Y, Zhou J, et al. Deep learning reconstruction at CT: Phantom study of the image characteristics. Acad Radiol [Internet]. 2020 Jan;27(1):82–7. doi: 10.1016/j.acra.2019.09.008. PubMed PMID: 31818389
46. Japan Society of Clinical Oncology. [Clinical Practice Guidelines for GIST, fourth edition] [Internet]. Tokyo: Japan Society of Clinical Oncology. 2023 Mar 3 [cited 2022 Aug 31]. Available from: http://www.jsco-cpg.jp/gist/guideline#I.html. Japanese.
47. Basree MM, Li C, Um H, et al. Leveraging radiomics and machine learning to differentiate radiation necrosis from recurrence in patients with brain metastases. J Neurooncol. 2024 Jun;168(2):307–16. Epub 2024 Apr 30. doi: 10.1007/s11060-024-04669-4. PubMed PMID: 38689115
48. Hu P, Chen L, Zhong Y, et al. Effects of slice thickness on CT radiomics features and models for staging liver fibrosis caused by chronic liver disease. Jpn J Radiol. 2022 Oct; 40(10):1061–8. Epub 2022 May 7. doi: 10.1007/s11604-022-01284-z. PubMed PMID: 35523919
49. Gupta S, Nayak K, Pendem S. Impact of slice thickness on reproducibility of CT radiomic features of lung tumors. F1000Res. 2023 Dec 1;12:1319. doi: 10.12688/f1000research.141148.2. PubMed PMID: 38454921; PubMed Central PMCID: PMC10918310
50. Zhao B, Tan Y, Tsai WY, et al. Reproducibility of radiomics for deciphering tumor phenotype with imaging. Sci Rep. 2016 Mar 24;6:23428. doi: 10.1038/srep23428. PubMed PMID: 27009765; PubMed Central PMCID: PMC4806325
51. Haider MA, Amitai MM, Rappaport DC, et al. Multidetector row helical CT in preoperative assessment of small (< or = 1.5 cm) liver metastases: is thinner collimation better? Radiology. 2002 Oct;225(1):137–42. doi: 10.1148/radiol.2251011225. PubMed PMID: 12354997
52. Cao L, Liu X, Qu T, et al. Improving spatial resolution and diagnostic confidence with thinner slice and deep learning image reconstruction in contrast-enhanced abdominal CT. Eur Radiol. 2023 Mar;33(3):1603–11. Epub 2022 Oct 3. doi: 10.1007/s00330-022-09146-y. PubMed PMID: 36190531
53. Xu JJ, Lonn L, Budtz-Jorgensen E, Jawad S, Ulriksen PS, Hansen KL. Evaluation of thin-slice abdominal DECT using deep-learning image reconstruction in 74 keV virtual monoenergetic images: an image quality comparison. Abdom Radiol (NY). 2023 Apr;48(4):1536–44. Epub 2023 Feb 21. doi: 10.1007/s00261-023-03845-w. PubMed PMID: 36810705
54. Lin X, Gao Y, Zhu C, et al. Improved overall image quality in low-dose dual-energy computed tomography enterography using deep-learning image reconstruction. Abdom Radiol (NY). 2024 Sep;49(9):2979–87. Epub 2024 Mar 14. doi: 10.1007/s00261-024-04221-y. PubMed PMID: 38480547
55. Lyu P, Li Z, Chen Y, et al. Deep learning reconstruction CT for liver metastases: low-dose dual-energy vs standard-dose single-energy. Eur Radiol. 2024 Jan;34(1): 28–38. Epub 2023 Aug 2. doi: 10.1007/s00330-023-10033-3. PubMed PMID: 37532899
56. Noda Y, Nakamura F, Yasuda N, et al. Advantages and disadvantages of single-source dual-energy whole-body CT angiography with 50% reduced iodine dose at 40 keV reconstruction. Br J Radiol [Internet]. 2021 May 1;94(1121): 20201276. Epub 2021 Feb 22. Available from: https://pmc.ncbi.nlm.nih.gov/articles/PMC8506171. doi: 10.1259/bjr.20201276. PubMed PMID: 33617294; PubMed Central PMCID: PMC8506171

(Received, August 19, 2024)
(Accepted, October 30, 2024)